JOURNAL OF Materials CHEMISTRY

On the structure of $Li_3Ti_2(PO_4)_3$

Abderrahim Aatiq,[a] Michel Ménétrier,*[b] Laurence Croguennec,[b] Emmanuelle Suard[c] and Claude Delmas[b]

[a]*Laboratoire de Chimie des Matériaux Solides, Faculté des Sciences Ben M'Sik, Avenue Idriss El harti, B.P. 7955 Casablanca, Morocco*
[b]*Institut de Chimie de la Matière Condensée de Bordeaux (ICMCB-CNRS) and Ecole Nationale Supérieure de Chimie et Physique de Bordeaux (ENSCPB), Université Bordeaux I, 87 avenue du Dr A. Schweitzer 33608 Pessac cedex, France. E-mail: menetrier@icmcb.u-bordeaux.fr*
[c]*Institut Laue-Langevin, rue des Martyrs, B.P. 156X, 38042 Grenoble cedex 9, France*

Received 15th April 2002, Accepted 29th July 2002
First published as an Advance Article on the web 27th August 2002

The structure of the Nasicon-type phase $Li_3Ti_2(PO_4)_3$, obtained by chemical lithiation of $LiTi_2(PO_4)_3$, has been characterised using neutron diffraction for the long range structure and ^{7}Li NMR for more local information. The lithium atoms were precisely located from the neutron diffraction data, using nuclear difference Fourier maps. The lithium ions, which were known to be in the large M2 cavity, occupy two M3 and M′3 subsites (distorted tetrahedra) with occupation factors of 2/3 and 1/3, respectively. From these two intermediate sites, it was shown that the diffusion pathway between two M1 sites in these Nasicon-type structures consists of a set of seven face-sharing tetrahedra. A variable temperature ^{7}Li MAS NMR study showed a set of signals due to a distribution of environments for a given Li^+ ion, in terms of occupied or vacant M3/M′3 sites in its vicinity. Elevation of the temperature to 353 K leads to a reversible exchange of these signals, due to fast hopping of Li between the two sites within a given M2 cavity.

Introduction

Since the discovery of the high conductivity of Nasicon-type materials by Hong[1] and Goodenough *et al.*,[2] a lot of studies have been devoted to these compounds.[3–12] Sodium-based compounds have been thoroughly investigated from both the structural and the electrical points of view.[1–3,7–9,12–16]

The crystal structure of Nasicon-type phases $A_xB_2(PO_4)_3$ exhibits a three-dimensional framework and allows for numerous ionic substitutions at various lattice sites. This framework is formed of corner-sharing PO_4 tetrahedra and BO_6 octahedra, leaving large interconnected channels which can be occupied by various A cations. Two main types of cavities, denoted M1 and M2, are generally considered. Within the Nasicon structure, each M1 cavity is situated between two BO_6 octahedra along the *c*-axis. Six M2 cavities with eightfold coordination are located between the $[O_3BO_3M1O_3BO_3\square O_3BO_3M1]_\infty$ ribbons and surround the M1 cavity.

Previous reports have shown that the Nasicon-type materials look promising as positive electrode materials for lithium batteries.[8,16–22] A long time ago (1987), some of us showed for the first time that lithium or sodium could be reversibly intercalated in the Nasicon framework by chemical and electrochemical intercalation in $LiTi_2(PO_4)_3$ and $NaTi_2(PO_4)_3$, respectively.[8,20] In the case of an $Li//Li_{(1+y)}Ti_2(PO_4)_3$ battery, the OCV curve $V(V) = f(y)$ shows a two-phase plateau at 2.5 V, which is attributed to the filling of the M2 cavity associated with cooperative migration of Li^+ ions from the M1 to the M2 site.[21] Interest also focused on voltage monitoring, as shown by the work of Quarton, Goodenough and Masquelier.[9–11,16–19] For a long time, it has been considered that the potential of these materials for application was limited due to their very low electronic conductivity, which somewhat impedes a high intercalation rate. Nevertheless, $LiFePO_4$ has recently been proposed as a material for positive electrode in lithium-ion batteries.[23] The limitations resulting from low intercalation–deintercalation kinetics have been solved using nanocomposite materials, such as $LiFePO_4$/C, that are characterised by a high exchange surface with the current collector.[24–26]

A few years ago, we undertook a general study of the Mn-Nasicon-type materials;[22–23,27–28] a comparative study of lithium intercalation in $LiTi_2(PO_4)_3$, $LiMn_{0.5}Ti_{1.5}Cr_{0.5}(PO_4)_3$, $Li_{0.5}Mn_{0.5}Ti_{1.5}Cr_{0.5}(PO_4)_3$ and $Mn_{0.5}Ti_2(PO_4)_3$ clearly illustrates that only the M2 cavities are involved in the intercalation for $Li_{0.5}Mn_{0.5}Ti_{1.5}Cr_{0.5}(PO_4)_3$ and $LiMn_{0.5}TiCr(PO_4)_3$. In the case of $Mn_{0.5}Ti_2(PO_4)_3$, the filling of half the initially empty M1 sites $\{[Mn_{0.5}\square_{0.5}]_{M1}Ti_2(PO_4)_3\}$ leads to a potential plateau in the vicinity of 2.8–3.0 V. Note that when the $[Li_{0.5}Mn_{0.5}]_{M1}$-$Ti_2(PO_4)_3$ composition is exceeded, the additional lithium ions are intercalated in the M2 cavity and a 2.5–2.2 V voltage range is obtained. This difference in cell voltage related to lithium intercalation in the M1 and M2 sites was also found in the $Li_yMn_{(0.5+x)}Ti_{(2-2x)}Cr_{2x}(PO_4)_3$ ($0 \leqslant x \leqslant 0.50$) system, where the number of lithium ions which can be intercalated in the vicinity of 3 V is equal to the number of vacancies $(0.5 - x)$ in the M1 site.[29] The presence of a jump in the OCV curve around the composition corresponding to complete occupation of the M1 site of $Li//Mn_{(0.5+x)}Ti_{(2-2x)}Cr_{2x}(PO_4)_3$ ($0 \leqslant x \leqslant 0.50$) systems shows how electrochemical intercalation can be used as a complementary structural characterisation for relevant structures, especially when other techniques lead to ambiguous results.[21–22,28–29] In all these studies, the "M2 site" is generally considered; however, its size is very large in comparison to the Li^+ ion radius, so that the exact position of the Li^+ ions is unknown.

By using neutron diffraction data, Boireau *et al.* showed that the lithium and copper atoms in $Li_{3.5}Cu_{0.5}Ti_2(PO_4)_3$ are distributed in the M2 cavity in two different positions denoted $M^1(2)$ and $M^2(2)$, these two sites being strongly distorted oxygenated tetrahedra connected through common corners and giving rise to six-membered rings around the M1 sites.[30] Later, in the Nasicon-type material with rhombohedral symmetry (space group $R\bar{3}$) of general formula

$Li_xM_xM'_{(2-x)}(SO_4)_{(3-y)}(SeO_4)_y$ ($0 \leqslant x \leqslant 0.5$ and $0 \leqslant y \leqslant 3$, with M = Mg, Ni, Zn, and M′ = Al, Cr), Slater *et al.* considered that lithium ions occupy only one of these two sites in the M2 cavity.[31] More recently, a neutron and X-ray diffraction investigation by Masquelier's group showed that in the two rhombohedral Nasicons $Li_3Fe_2(PO_4)_3$ and $Li_3V_2(PO_4)_3$, which were prepared by ion exchange of $Na^+ \leftrightarrow Li^+$ from $Na_3Fe_2(PO_4)_3$ and $Na_3V_2(PO_4)_3$, respectively, lithium ions occupy only one crystallographic site in the 18f general position of the $R\bar{3}$ space group.[18,19] In this latter site, which was denoted M3 for the first time by these authors, the lithium atoms surround only the empty M1(3a) site and are arranged in a tetrahedral environment, similar to one of those found in 1993 by Boireau *et al.* in $Li_{3.5}Cu_{0.5}Ti_2(PO_4)_3$. This M3 site gives rise to one signal in the ^6Li NMR spectrum at room temperature.[18,19] Note that for $Li_3Fe_2(PO_4)_3$, the suspicion of a mobility effect due to Li^+ hopping was mentioned by the authors.[18]

In our group, a preliminary X-ray diffraction study showed a strong modification of the diffraction patterns upon lithium intercalation in $LiTi_2(PO_4)_3$, suggesting a strong modification of the Li^+ ion distribution in the structure.[20] By using neutron diffraction data, a preliminary structural refinement showed that the lithium atoms in $Li_3Ti_2(PO_4)_3$ are within the M2 cavity of the Nasicon structure.[20] A comparative ^7Li MAS NMR study for the two end members of the $LiTi_2(PO_4)_3$–$Li_3Ti_2(PO_4)_3$ system, described in the second part of this paper, shows the presence of several signals for $Li_3Ti_2(PO_4)_3$, which suggest different Li environments within the structure. Therefore, in order to precisely locate the positions of the lithium ions within the $[Ti_2(PO_4)_3]$ framework, the structural characterisation by X-ray and neutron diffraction has been reconsidered, as well as the NMR characterisation in the 296–253 K range, in order to obtain complementary information about the short range structure of both $LiTi_2(PO_4)_3$ and $Li_3Ti_2(PO_4)_3$.

Experimental

$LiTi_2(PO_4)_3$ was obtained by solid state reaction of stoichiometric amounts of Li_2CO_3, TiO_2 and $NH_4H_2PO_4$. The starting materials were finely ground and then heated progressively between 200 and 1000 °C in air.

$Li_3Ti_2(PO_4)_3$ can be obtained, at room temperature, by chemical or electrochemical lithium intercalation. For chemical intercalation, n-butyllithium (in excess) was initially diluted in dry hexane and then added under stirring to $LiTi_2(PO_4)_3$ dispersed in hexane, within an argon filled glove box. The product was then washed with dry hexane and finally dried under vacuum. Electrochemical intercalation was carried out in lithium cells with the following electrochemical chain: $Li/LiClO_4$ (1 M) (in propylene carbonate)/Nasicon (70 wt%) + graphite (28 wt%) + polytetrafluoroethylene (2 wt%). The cells, assembled in an argon filled dry box, were discharged at room temperature under low current density (*C*/40) *via* a home-made cycling system managed by an HP 1000 computer.[32] For the OCV experiments, in order to be as close as possible to the equilibrium conditions, the relaxation was interrupted when the slope of the $V = f(t)$ curve was less than 1 mV h^{-1}.

The X-ray diffraction data were collected at room temperature with a Philips PW 1820 diffractometer (Cu-Kα) equipped with a diffracted beam monochromator. The data were collected in the 5–120° (2θ) range with a step width of 0.02° (2θ) and a step time of 40 s. The neutron powder diffraction data were collected on the high-resolution powder diffractometer D2B of the Institut Laue-Langevin. The samples were contained in vanadium cans of 8 mm diameter and 5 cm height. The diffraction patterns (λ = 1.59417 Å) were collected at room temperature and at 350 K, respectively, from 0 to 162° (2θ) with an 0.05° (2θ) step. All the diffraction data were analyzed using the Rietveld refinement method.[33]

NMR spectra were recorded with a Bruker MSL 200 spectrometer operating at 77.7 MHz for ^7Li and 81 MHz for ^{31}P. The samples were packed in a 4 mm zirconia rotor and spinning speeds up to 15 kHz were used. Single (90°) pulse sequences around 3.5 μs duration were employed with a delay of 10 s between pulses. The spectra were recorded between 296 and 353 K. The chemical shift values are given with respect to an 85% H_3PO_4 solution for ^{31}P NMR spectra and a 1 M LiCl solution for ^7Li NMR spectra.

Results

The electrochemical intercalation study was carried out using an $Li//LiTi_2(PO_4)_3$ cell. As already reported by some of us, the OCV curve shows a two-phase plateau at 2.50 V [Fig. 1(a)] which is attributed to the formation of $Li_3Ti_2(PO_4)_3$ and, therefore, associated with lithium intercalation in the M2 cavity of $LiTi_2(PO_4)_3$.[8,20–22]

The lithium electrochemical intercalation–deintercalation study of $Li_3Ti_2(PO_4)_3$ was carried out in two steps. After a first charge up to 3.5 V, a cycling experiment was performed for an $Li//Li_3Ti_2(PO_4)_3$ cell at low rate (*C*/40) between 2.2 and 3.5 V [Fig. 1(b)]. During the first charge, 1.7 lithium atoms per formula unit are deintercalated from the structure. The observed charge–discharge reversibility clearly shows that the structural integrity of the $Ti_2(PO_4)_3$ Nasicon skeleton is maintained. In the second experiment, a continuous discharge of the $Li//Li_3Ti_2(PO_4)_3$ cell was attempted. In this case, a rapid jump in the $V = f(y)$ curve is observed, from 2.5 to 1 V, showing that no further lithium can be intercalated in this phase.

A preliminary structural characterisation of both end members, $LiTi_2(PO_4)_3$ and $Li_3Ti_2(PO_4)_3$, showed a large

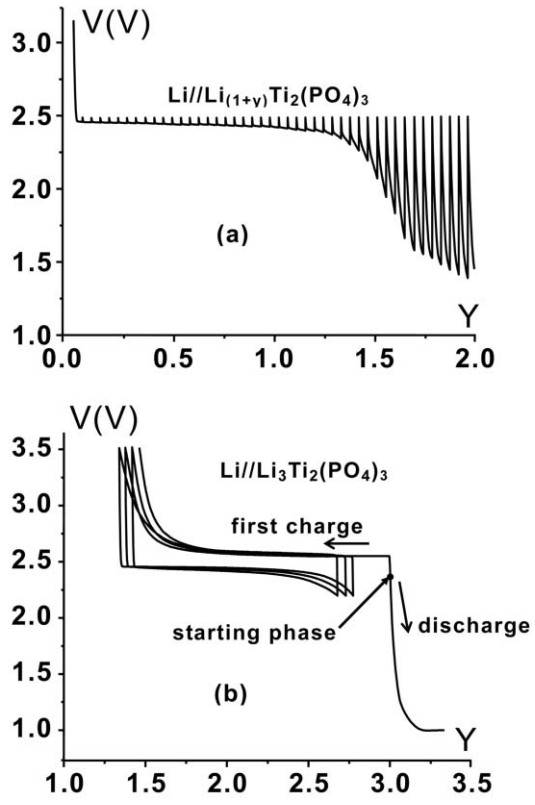

Fig. 1 (a) OCV discharge curve for an $Li//LiTi_2(PO_4)_3$ cell (*C*/40 over periods of 1 h, criterion for the end of relaxation: $dV/dt \leqslant 1$ mV h^{-1}), (b) Cycling of an $Li//Li_3Ti_2(PO_4)_3$ cell between 2.2–3.5 V (*C*/40) and first discharge curve for an $Li//Li_3Ti_2(PO_4)_3$ cell (*C*/40).

increase in the c_{hex} parameter upon lithium intercalation.[20] In order to understand this unexpected behavior, an in-depth structural characterisation of $LiTi_2(PO_4)_3$ and $Li_3Ti_2(PO_4)_3$ was undertaken.

Structural refinement

The refinement of the $LiTi_2(PO_4)_3$ and $Li_3Ti_2(PO_4)_3$ structures was done using the Rietveld analysis of their X-ray and neutron diffraction patterns. The localisation of Li atoms using the X-ray diffraction technique is not efficient due to their low X-ray scattering factor. Therefore, from the X-ray data, only the atomic positions of Ti, P and O atoms within the framework can be refined, whereas the neutron diffraction technique can also give accurate information about the lithium atomic positions.

$LiTi_2(PO_4)_3$. The X-ray powder diffraction data show that $LiTi_2(PO_4)_3$ crystallises in the rhombohedral system (space group $R\bar{3}c$), with a_{hex} = 8.5110(1) and c_{hex} = 20.843(4) Å. Assuming that $LiTi_2(PO_4)_3$ is isostructural with $NaZr_2(PO_4)_3$,[13] the Ti, P and O atoms are in the (12c), (18e) and (36f) Wyckoff positions, respectively, of the $R\bar{3}c$ space group. Li was assumed to occupy the M1 site [*i.e.* the (6b) position]. This refinement led to a rather good agreement between the experimental and the calculated XRD patterns (Fig. 2) and to low reliability factors (R_{wp} = 13%; R_B = 4.2%). It appears, thus, that this structural model describes the structure of $LiTi_2(PO_4)_3$ rather well. Nevertheless, in order to confirm the position of lithium atoms in the structure, the $LiTi_2(PO_4)_3$ neutron diffraction pattern was also recorded at room temperature. The Rietveld analysis of these neutron diffraction data was performed in three steps. In the first step, only the $Ti_2(PO_4)_3$ framework was considered. Then, the Fourier difference technique was used to localise the lithium atoms in the structure: it reveals only significant residual nuclear densities at the M1 site [(6b) position], confirming that only the M1 site is occupied by the lithium ions in $LiTi_2(PO_4)_3$. Finally, the isotropic atomic displacement factors were refined. The cell parameters and the atomic positions determined are given in Table 1, they are in very close agreement with those calculated from the XRD data. This structural hypothesis also leads to a good agreement between the experimental and calculated neutron diffraction patterns and to low reliability factors (R_{wp} = 9.8%; R_B = 4.0%). Note that due to the large size of the M1 site, a large B_{iso} value is, as expected, obtained for the Li atoms (4.8 Å^2) (Table 1).

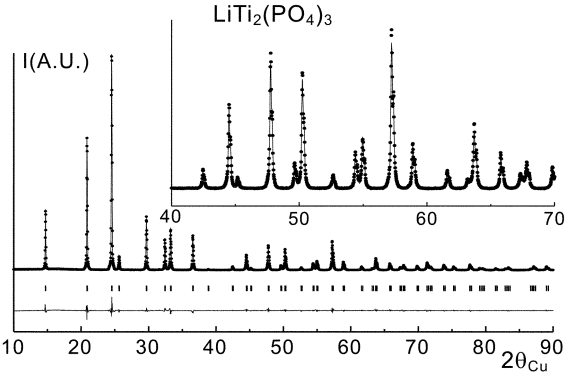

Fig. 2 Comparison of the experimental (●) and calculated (—) X-ray diffraction patterns for $LiTi_2(PO_4)_3$. The positions of the (*h k l*) reflections and the difference curve are also given.

The Li–O2 distance [2.266(5) Å] is significantly larger than expected from the sum of the ionic radii,[34] but similar, as expected, to that found in $LiGe_2(PO_4)_3$ [2.21(1) Å][35] and much smaller than that found in $LiZr_2(PO_4)_3$ [2.49(1) Å].[12] Indeed, it is well known that in $LiB_2(PO_4)_3$ (B = Ge, Ti, Zr), when the size of the B cation increases ($r_{Ge^{4+}}$ = 0.53, $r_{Ti^{4+}}$ = 0.605 and $r_{Zr^{4+}}$ = 0.72 Å in octahedral environments), the volume of the M1 site increases and, therefore, the Li–O distances increase. The P–O distances (~1.5 Å) are regular and close to those typically observed in Nasicon phosphates. The Ti–O distances [1.88(1), 1.98(1) Å] show a [3 + 3] distortion of the TiO_6 octahedra.

$Li_3Ti_2(PO_4)_3$. The X-ray powder diffraction data show that $Li_3Ti_2(PO_4)_3$ crystallises in the rhombohedral system with a_{hex} = 8.3828(6) and c_{hex} = 22.873(2) Å.

The extinction rules observed are not consistent with the $R\bar{3}c$ space group, commonly used to describe the Nasicon-type structures. Indeed, the presence of the (003) and (101) diffraction lines in the XRD pattern is incompatible with a *c*-axis glide plane. Three space groups appear to be consistent with the observed XRD data: *R*32, $R\bar{3}$ or *R*3.

A preliminary structural refinement of the X-ray powder diffraction data in the three possible space groups showed that the best agreement is obtained in the $R\bar{3}$ space group. Using the XRD data, only the $Ti_2(PO_4)_3$ framework was refined, with the Ti atoms in the (6c) position and the P and O atoms in (18f). The structural parameters calculated previously for $LiTi_2(PO_4)_3$ were used as starting parameters. This refinement leads to low reliability factors (R_{wp} = 13%; R_B = 4.5%) and good minimisation of the difference between the experimental and the calculated XRD patterns. Then, a Rietveld analysis of the neutron diffraction data was performed in order to localise the Li atoms in the structure. The Fourier difference technique revealed that residual nuclear densities remain at two different 18f positions; they correspond to the $M^1(2)$ (or M3) and $M^2(2)$ sites discussed in the introduction: we denote them M3 and M′3, respectively. Lithium was thus introduced in the structure at these positions, and the atomic coordinates and occupation factors associated with these positions were refined. It appeared that convergence was achieved for occupancy factors close to 2/3 and 1/3 for M3 and M′3, respectively. Note that the occupation ratios converge to these values, whether the total Li amount in the material is constrained or not to be equal to 3. As shown in Fig. 3 and in Table 2, a good agreement is

Table 1 Results obtained from the refinement of the neutron diffraction pattern[a] of $LiTi_2(PO_4)_3$[b] by the Rietveld method[c]

Atom	Site	Wyckoff position			B_{iso}/Å^2	Occupancy	Bond length/Å
Li	6b	0	0	0	4.8(9)	1	Li–O2 2.266(5) × 6
Ti	12c	0	0	0.1421(6)	0.7(1)	1	Ti–O1 1.880(9) × 3
							Ti–O2 1.977(9) × 3
P	18e	0.2903(7)	0	¼	0.5(1)	1	P–O1 1.528(6) × 2
							P–O2 1.527(6) × 2
O1	36f	0.1850(6)	0.9960(7)	0.1901(1)	0.94(6)	1	
O2	36f	0.1884(6)	0.1641(5)	0.0810(2)	0.69(6)	1	

[a]Conditions of the run: λ = 1.59417 Å, *T* = 300 K, Angular range 0 ⩽ 2θ ⩽ 162°, 2θ increment = 0.05°, zero point (2θ) = 0.036(2), absorption correction (μR) = 0.112, no. fitted parameters = 29. Profile parameters: profile function Pseudo-Voigt PV = $\eta L + (1-\eta)G$; $\eta = \eta_0 + X(2\theta)$ [η_0 = 0.14(3), *X* = 0.0018(5)]; halfwidth parameters *U* = 0.028(2), *V* = −0.064(3), *W* = 0.069(2). [b]Space group $R\bar{3}c$; a_{hex} = 8.5110(1), c_{hex} = 20.843(4) Å. [c]R_{wp} = 9.8%, R_B = 3.99%.

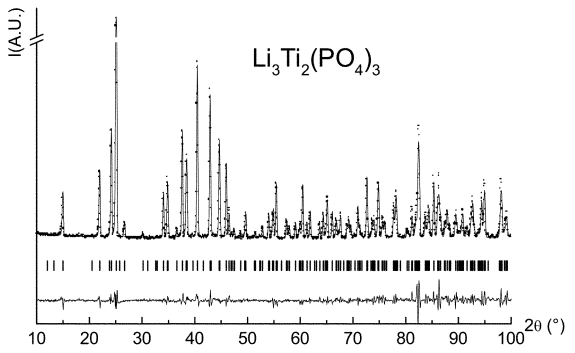

Fig. 3 Comparison of the experimental (●) and calculated (—) neutron diffraction patterns for $Li_3Ti_2(PO_4)_3$. The position of the (*h k l*) reflections and the difference curve are also given.

obtained between the experimental and calculated neutron diffraction patterns, and also good reliability factors (R_{wp} = 17.8%; R_B = 7.52%) are observed. Note that the structural parameters obtained from the neutron diffraction data are, as expected, similar to those obtained from the XRD data. The difference Fourier maps (sections perpendicular to the *c*-axis, with $z = 0.0435$ and 0.1196) are displayed in Fig. 4. They show the positions of the M3 and M′3 sites relative to the ribbons.

Structural description of $Li_3Ti_2(PO_4)_3$. As shown by the neutron diffraction data, the Li^+ ions occupy corners (denoted M3 and M′3) of the large 8–10-fold coordinated cavity (M2) (Fig. 5). In the M3 and M′3 sites, the Li atoms appear to be in very distorted tetrahedral environments [Fig. 6(a)]. Note that due to the small Li_{M3}–$Li_{M'3}$ distance (1.69 Å), adjacent M3 and M′3 sites are probably not occupied simultaneously. Nevertheless, in $Li_{3.5}Cu_{0.5}Ti_2(PO_4)_3$, adjacent M3 and M′3 sites are occupied simultaneously with an M3–M′3 distance of 2.05 Å.[30]

The $Li_{M3}O_4$ units are linked through corners, by O(4) oxygen atoms, to form $[Li_6]_{M3}O_{18}$ six-membered rings which lie in the (*a*, *b*) plane and surround only the empty M1(3a) site [Fig. 6(a)]. The shortest Li_{M3}–Li_{M3} distances within an $[Li_6]_{M3}O_{18}$ ring are 3.288(2) Å, in good agreement with the possible occupancy of two neighbouring tetrahedral sites belonging to the same ring. Each $Li_{M3}O_4$ tetrahedron shares one corner with a $Ti(1)O_6$ octahedron [*via* an O(1) oxygen], an edge [O(2)–O(4)] with a $Ti(2)O_6$ octahedron and a corner [*via* the second O(4)] with another $Ti(2)O_6$ octahedron [Fig. 6(b)]. Thus, the Li_{M3} ions have different interactions with the three TiO_6 octahedra to which they are connected. Note that this point is important to explain the NMR results presented in the following.

The $Li_{M'3}$ atoms are present in even more distorted

Table 2 Results obtained from the refinement of the neutron diffraction pattern[a] of $Li_3Ti_2(PO_4)_3$[b] by the Rietveld method.[c] The atomic positions and isotropic displacement factors obtained from the refinement of the X-ray diffraction pattern are given in italics for comparison

Atom	Site	Wyckoff position			B_{iso}/Å^2	Occupancy
Li1 (M3)	18f	0.030(4)	0.319(4)	0.045(1)	1.2(6)	0.72(6)
Li2 (M′3)	18f	0.055(8)	0.373(9)	0.117(3)	1.2(6)	0.34(6)
Ti1	6c	0	0	0.145(1)	1.0(5)	1
		0	*0*	*0.1447(2)*	*0.23(1)*	
Ti2	6c	0	0	0.3483(8)	0.4(2)	1
		0	*0*	*0.3470(2)*	*−0.07(1)*	
P	18f	0.291(1)	−0.001(1)	0.2501(4)	0.8(4)	1
		0.2904(4)	*−0.0027(7)*	*0.2510(2)*	*0.40(5)*	
O1	18f	0.167(1)	0.216(1)	0.0899(4)	1.3(6)	1
		0.1620(9)	*0.2187(8)*	*0.0896(3)*	*1.2(2)*	
O2	18f	0.136(1)	0.229(1)	0.3982(4)	1.1(6)	1
		0.123(1)	*0.228(7)*	*0.398(2)*	*0.9(1)*	
O3	18f	0.197(1)	0.992(1)	0.1932(4)	1.9(9)	1
		0.192(1)	*0.988(1)*	*0.192(3)*	*1.2(2)*	
O4	18f	0.911(1)	0.145(1)	0.2990(4)	1.8(9)	1
		0.904(1)	*0.147(1)*	*0.299(2)*	*1.2(2)*	

[a]Conditions of the run: λ = 1.59417 Å, T = 300 K, Angular range $0 \leqslant 2\theta \leqslant 162°$, 2θ increment = 0.05°, zero point (2θ) = 0.047(4), absorption correction (μR) = 0.192, no. fitted parameters = 51. Profile parameters: profile function Pseudo-Voigt PV = $\eta L + (1-\eta)G$; $\eta = \eta_0 + X(2\theta)$ [η_0 = 0.34(4), X = −0.0040(9)]; halfwidth parameters U = 0.11(1), V = −0.11(1), W = 0.081(4). [b]Space group $R\bar{3}$; a_{hex} = 8.3828(6), c_{hex} = 22.873(2) Å. [c]R_{wp} = 17.8%, R_B = 7.52%.

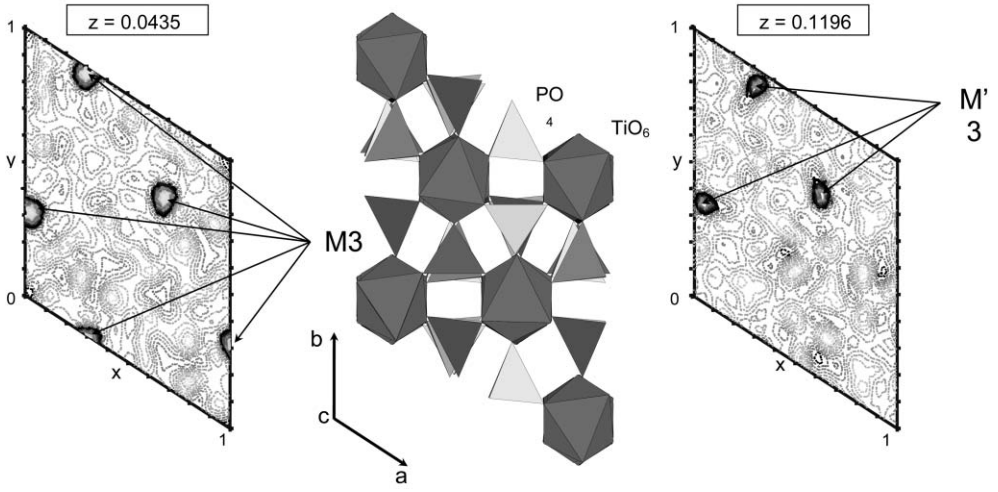

Fig. 4 Difference Fourier maps showing the residual nuclear density in planes parallel to the (001) plane at z = 0.0435 and 0.1196. A projection of the structure in the (001) plane is also given, in order to show the position of the ribbons.

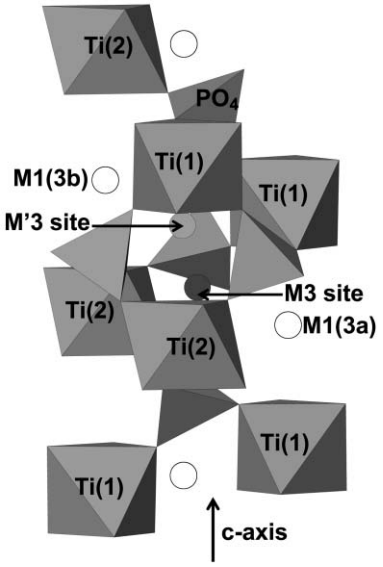

Fig. 5 View of the $Li_3Ti_2(PO_4)_3$ structure along the *c*-axis: the M3 and M′3 positions are given within the M2 cavity.

tetrahedral environments, as shown by the Li–O distances and O–Li–O angles reported in Table 3. Note that these LiO_4 tetrahedra are almost flat. The $Li_{M'3}O_4$ units are also linked through corners, by O(3) oxygen atoms, to form $[Li_6]_{M'3}O_{18}$ six-membered rings in the (*a*, *b*) plane and surround only the M1(3b) site [Fig. 6(a)]. The shortest $Li_{M'3}$–$Li_{M'3}$ distances within the $[Li_6]_{M'3}O_{18}$ ring are 3.306(2) Å. Each $Li_{M'3}O_4$ tetrahedron shares one corner with a $Ti(2)O_6$ octahedron [*via* an O(2) oxygen], an edge [O(1)–O(3)] with a $Ti(1)O_6$ octahedron and a corner [*via* the second O(3)] with another $Ti(1)O_6$ octahedron [Fig. 6(b)]. From a general point of view, the same behavior as for Li_{M3} is observed, with different interactions with the three TiO_6 octahedra to which they are connected.

As shown in Table 3, the Ti–O interatomic distances are in good agreement with the reduction of Ti(IV) to Ti(III) upon lithium intercalation. Indeed, an increase in the Ti–O distances is observed for $Li_3Ti_2(PO_4)_3$ in comparison to what is observed for $LiTi_2(PO_4)_3$. Moreover, the TiO_6 octahedra in $Li_3Ti_2(PO_4)_3$ exhibit six almost similar Ti–O distances, and are less distorted than in $LiTi_2(PO_4)_3$, where LiO_6 (M1) and TiO_6 share faces. The P–O distance values in $Li_3Ti_2(PO_4)_3$ (1.51–1.55 Å) are also in good agreement with those typically observed in Nasicon-like phosphates.

Close examination of the atomic positions and interatomic distances shows that the main difference between the $LiTi_2(PO_4)_3$ and $Li_3Ti_2(PO_4)_3$ structures is in the ribbons parallel to the *c*-axis. The large increase in the c_{hex} parameter upon lithium intercalation in $LiTi_2(PO_4)_3$ is due to the removal of the lithium ions from the M1 site. Indeed, they no longer play the role of screening ions between the oxygen layers that are on either side of the M1 cavity. As shown in Fig. 6(b), three Ti–Ti distances [Ti(1)–Ti(1), Ti(1)–Ti(2) and Ti(2)–Ti(2)] are observed in $Li_3Ti_2(PO_4)_3$ within a given ribbon along the *c*-axis. Note that the Ti(2)–Ti(2) interatomic distances [6.94(1) Å] are much longer than the Ti(1)–Ti(1) ones [6.61(1) Å] [Fig. 6(b)]. The corresponding Ti–Ti distance in $LiTi_2(PO_4)_3$ is only 5.91 Å, due to the large screening power of the lithium ions in the M1 site. The Ti(1)–Ti(2) distance between adjacent octahedra varies to a smaller extent between $LiTi_2(PO_4)_3$ [4.51(1) Å] and $Li_3Ti_2(PO_4)_3$ [4.66(1) Å]; indeed, both TiO_6 octahedra belong to the same $Ti_2(PO_4)_3$ lantern. The size modification of the M1 site in $Li_3Ti_2(PO_4)_3$ is accompanied by oxygen displacements perpendicular to the *c*-axis, which give rise to a rotation of the PO_4 tetrahedra and thus lead to a distortion of the $[Ti_2(PO_4)_3]$ framework.

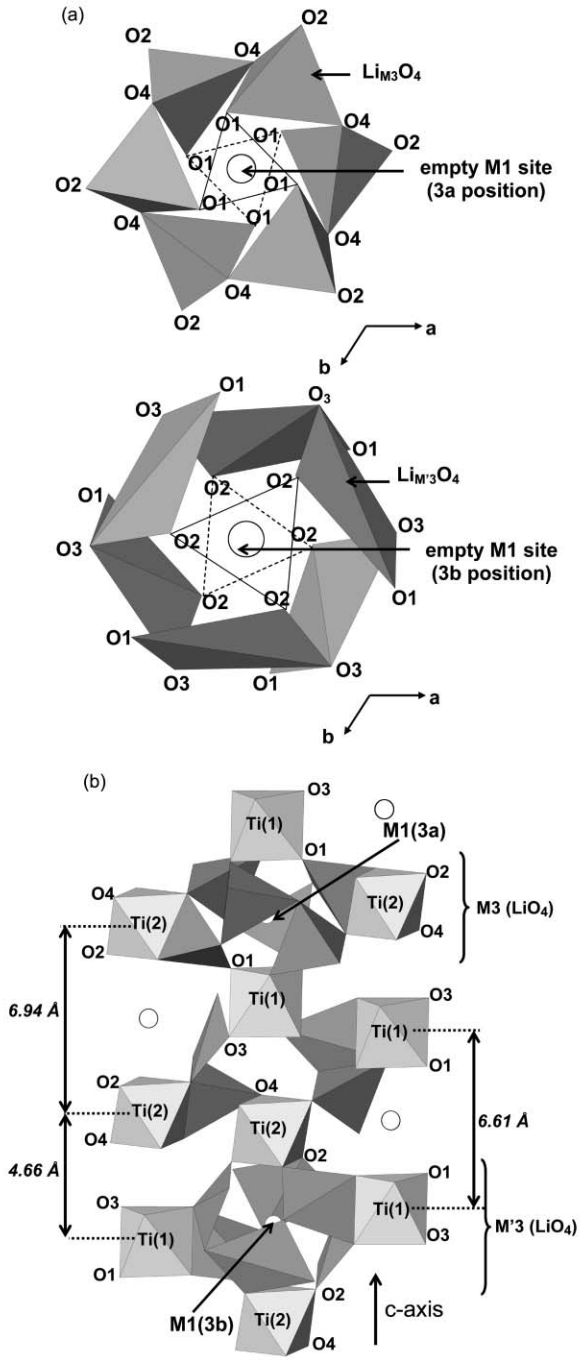

Fig. 6 (a) Linking of $Li_{M3}O_4$ and $Li_{M'3}O_4$ polyhedra in $Li_3Ti_2(PO_4)_3$ to form rings around empty M1(3a) and M1(3b) sites, respectively. The triangles correspond to the faces of the TiO_6 octahedra which are at opposite sides (— and - - -) of the M1 sites [$Ti(1)O_6$ for M1(3a) and $Ti(2)O_6$ for M1(3b)]. (b) View of the $Li_3Ti_2(PO_4)_3$ structure along the *c*-axis, with the $[Li_6]_{M3}O_{18}$ and $[Li_6]_{M'3}O_{18}$ six-membered rings around the M1(3a) and M1(3b) sites, respectively.

It is well known that in the Nasicon structure, the long distance migration of alkali metal ions must follow the path M1 → M2 → M1 → M2, *etc.* The M3 and M′3 sites being included within the M2 cavity (slightly shifted *vs.* its centre of ∼ ±0.9 Å along the *c*-axis direction), they necessarily play an important role in the diffusion process. Considering the structure, it appears that the lithium ions can diffuse between the M1(3a), M3, M′3 and M1(3b) sites *via* a set of seven face-sharing tetrahedra (Fig. 7). In the following diffusion pathway, the faces shared between two adjacent tetrahedra are given in brackets: **M1(3a)** (ABC) ADCB (ACD) ACDE (CDE) **CFED(M3)** (CEF) CFEH (CFH) **CHFG(M′3)** (FGH) FGHJ (FGJ) IGFJ (FIJ) **M1(3b)**. Such a diffusion path allows the

Table 3 Interatomic distances (Å) and O–Li–O′ angles (°) calculated for $Li_3Ti_2(PO_4)_3$

$Li1_{M3}$–O1	2.02(4)	O1–$Li1_{M3}$–O2	114(1)
$Li1_{M3}$–O2	1.95(4)	O2–$Li1_{M3}$–O4	86(1)
$Li1_{M3}$–O4	2.01(4)	O4–$Li1_{M3}$–O4	115(1)
$Li1_{M3}$–O4	2.17(4)	O4–$Li1_{M3}$–O1	125(1)
$Li2_{M'3}$–O1	2.05(8)	O1–$Li2_{M'3}$–O2	114(1)
$Li2_{M'3}$–O2	1.93(7)	O2–$Li2_{M'3}$–O3	66(1)
$Li2_{M'3}$–O3	2.15(7)	O3–$Li2_{M'3}$–O3	101(1)
$Li2_{M'3}$–O3	2.53(8)	O3–$Li2_{M'3}$–O1	79(1)
Ti1–O1 (×3)	2.07(2)		
Ti1–O3 (×3)	2.02(2)		
Ti2–O2 (×3)	2.03(1)		
Ti2–O4 (×3)	2.05(1)		
P–O1	1.53(1)		
P–O2	1.54(1)		
P–O3	1.51(1)		
P–O4	1.55(1)		

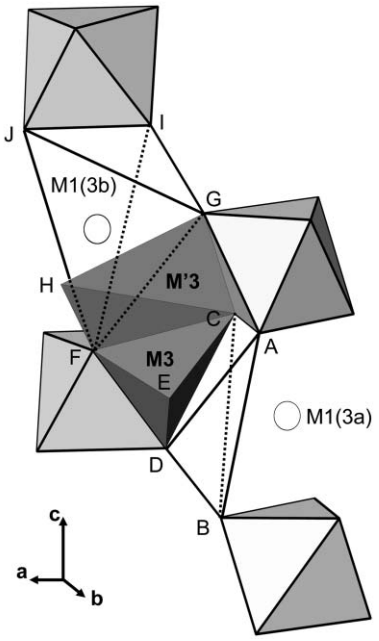

Fig. 7 Diffusion path for the lithium ions in the $Li_3Ti_2(PO_4)_3$ structure, between the M1(3a), M3, M′3 and M1(3b) sites.

formation of $Li_3Ti_2(PO_4)_3$ from $LiTi_2(PO_4)_3$ upon electrochemical intercalation at room temperature to be explained . The distortion of the lithium environments (M3 and M′3) in this structure must make Li ions rather unstable in these sites and must, therefore, promote their mobility at high temperature. Indeed, high mobility between the M3 and M′3 sites was shown by ^{7}Li NMR, as discussed in the following section. This diffusion pathway is likely to be general for all Nasicon structures.

In order to obtain more short-range structural information about the distribution of Li atoms, a ^{7}Li and ^{31}P MAS NMR study of the $LiTi_2(PO_4)_3$ and $Li_3Ti_2(PO_4)_3$ compounds was undertaken.

MAS NMR Study

The ^{31}P MAS NMR spectrum of $LiTi_2(PO_4)_3$ shows only one narrow signal in the chemical shift range of diamagnetic phosphates [Fig. 8(a)]. So does the ^{7}Li MAS NMR spectrum, with a spinning side band pattern characteristic of a quadrupolar interaction due to the non-spherical symmetry of the electrical field gradient at the Li site [Fig. 8(b)]. These data are consistent with the presence of Li ions only in the M1 site.

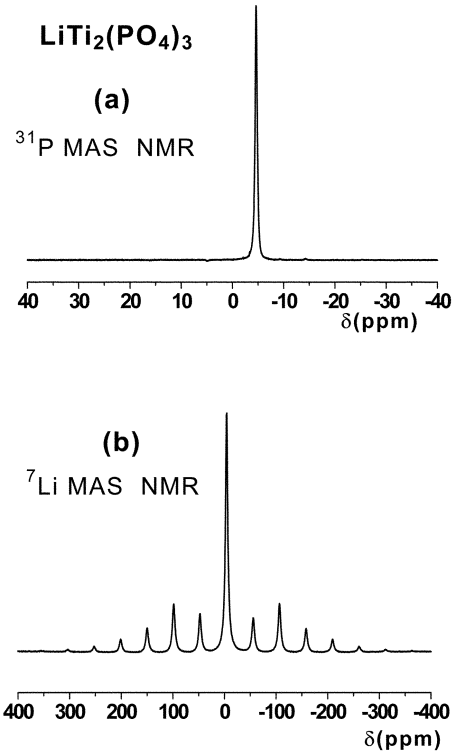

Fig. 8 ^{31}P MAS NMR spectrum (a) and ^{7}Li MAS NMR spectrum (b) of $LiTi_2(PO_4)_3$.

The ^{7}Li MAS NMR spectrum of $Li_3Ti_2(PO_4)_3$ at room temperature shown in Fig. 9 is considerably broader than that of $LiTi_2(PO_4)_3$. This results mostly from a hyperfine interaction due to the paramagnetic Ti^{3+} ions, which leads to a strong electron–nucleus dipolar interaction. Furthermore, the second aspect of the hyperfine interaction is the transfer of some density of a single electron from the Ti^{3+} t_{2g} orbital to the site (2 s orbital) of the Li nucleus, which leads to a Fermi contact shift of the NMR signal *vs.* $LiTi_2(PO_4)_3$. However, the most striking feature of the spectrum is the presence of a whole set of signals, which can be better observed in Fig. 10, where only the isotropic signals are shown. Since the structural characterisation described above shows two crystallographic sites (M3 and M′3), occupied by Li^+ with 2/3 and 1/3 occupation ratios, respectively, one would have expected two ^{7}Li NMR signals. Indeed, the oxygen and titanium environments are different for the two cases, which must lead to different geometries for the orbital overlaps and, therefore, to different Fermi contact shifts for the two types of lithium. The set of NMR signals observed must, therefore,

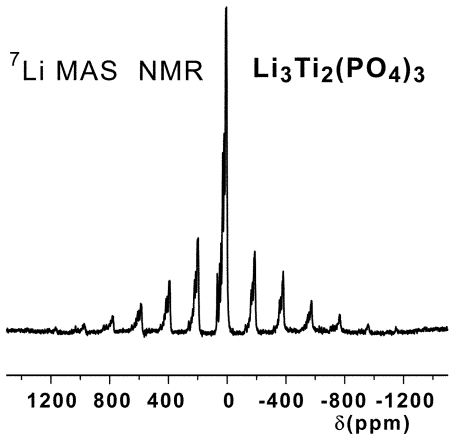

Fig. 9 ^{7}Li MAS NMR spectrum of $Li_3Ti_2(PO_4)_3$ at 296 K.

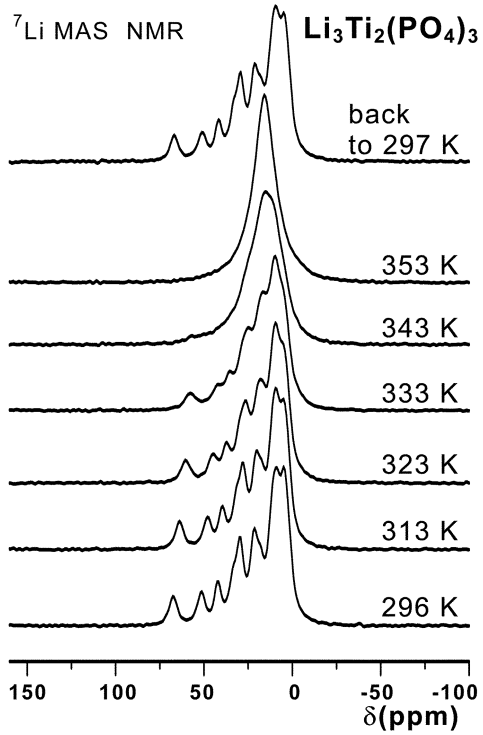

Fig. 10 ^{7}Li MAS NMR spectra of $Li_3Ti_2(PO_4)_3$ in the 296–353 K temperature range.

arise from the additional effect, on a given lithium ion, of the nature of the sites (*i.e.* M3 or M′3) occupied by lithium in the neighbouring M2 cavities. The occupation of M3 or of M′3 can indeed entail slight but significant changes in the position of the Ti^{3+} ions in the neighbouring TiO_6 octahedra (one shares an edge, and two others a corner with the tetrahedral M3 or M′3 site), which will alter the contact shift caused by these Ti^{3+} ions on their adjacent Li ions (each TiO_6 shares edges with three M3 or M′3 sites, and corners with three others). Therefore, a distribution of NMR signals for each type of Li ion (in M3 and in M′3) should correspond to the expected distribution in the occupation of the M3 or M′3 sites in the M2 cavities "sharing" a TiO_6 octahedron with the Li site considered. Although the mechanism of electron spin density transfer is not known, it is tempting to draw a very crude scheme of the situation expected. It is first reasonable to consider that each Li^+ ion is most influenced by the Ti^{3+} ion with which it shares an edge, since this allows a proper geometry for a direct $Ti(t_{2g})$–Li(2 s) overlap through the common edge. In turn, this Ti^{3+} ion shares edges with two other M3 or M′3 sites, which can be occupied or empty, leading to four possible situations. Considering that each of these situations leads to a slightly different atomic position for this Ti^{3+} ion, and therefore to a different contact shift on the original Li, we have a set of four NMR signals. Since this should hold, but with a different shift, for Li in both the M3 and the M′3 site, a total of 8 lines could be assumed, which is not far from the observation.

Fig. 10 shows that a slight increase in temperature leads to a perfectly reversible merging of these signals. This is a classical exchange phenomenon, assigned to a mobility of the Li^+ ions, within a given M2 cavity, between the M3 and M′3 sites through the intermediate CFEH tetrahedral site, as discussed earlier and shown in Fig. 7. When the Li hopping rate between the two positions becomes faster than the difference in NMR shifts of the individual signals, expressed in Hz (*i.e.* ~5 kHz), there is not enough time for the FID (free induction decay) of each individual signal to be recorded. This is the NMR exchange phenomenon, which leads to the observation of a single signal at the barycentre of the set of individual signals.

In order to characterise the effect of the same temperature change on the diffraction patterns, we have also recorded the neutron diffraction pattern of $Li_3Ti_2(PO_4)_3$ at 350 K, which shows no significant change as compared to the room temperature one. In contrast to NMR, the time scale of neutron diffraction is extremely short and, during signal accumulation, a very large number of instantaneous pictures are added, in which Li^+ ions are mostly in their sites, in-between two hops, which leads to observation of an averaged situation with the 2/3 and 1/3 occupation ratios in the M3 and M′3 sites. The slight change in the Li hopping rate between room temperature and 350 K should not, therefore, alter this observation. A much larger change in the hopping rate would probably be necessary for the diffraction to observe a significant number of Li^+ ions during their hop, that is in-between their two crystallographic sites.

The ^{31}P MAS NMR spectrum of $Li_3Ti_2(PO_4)_3$ shown in Fig. 11 exhibits a very complex set of signals, again resulting from hyperfine interactions due to Ti^{3+}. Since a single crystallographic type of phosphorus exists in the structure, this also supports the hypothesis that the Ti and/or P atoms are influenced by the distribution in the occupation of the M3/M′3 sites by the neighbouring Li ions, which alters the contact shift on ^{31}P.

We have also recorded the ^{7}Li MAS NMR signal of $Li_{2.80}Mn_{0.10}Ti_2(PO_4)_3$ (chemically synthesised from $Li_{0.80}Mn_{0.10}Ti_2(PO_4)_3$ with excess n-butyllithium), which is shown in Fig. 12 for comparison with that of $Li_3Ti_2(PO_4)_3$. It is striking that this spectrum exhibits a set of individual signals very similar to that for $Li_3Ti_2(PO_4)_3$, although with additional bandwidth due to the presence of the paramagnetic Mn^{2+} ions. It therefore seems that the relative occupancy of the M3 and M′3 sites in the two materials obeys very similar ordering schemes.

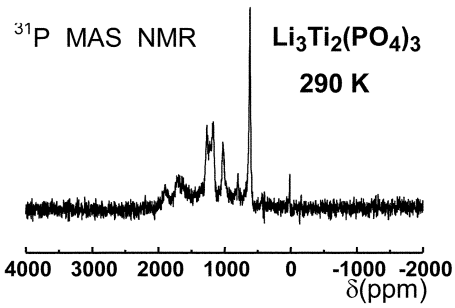

Fig. 11 ^{31}P MAS NMR spectrum of $Li_3Ti_2(PO_4)_3$.

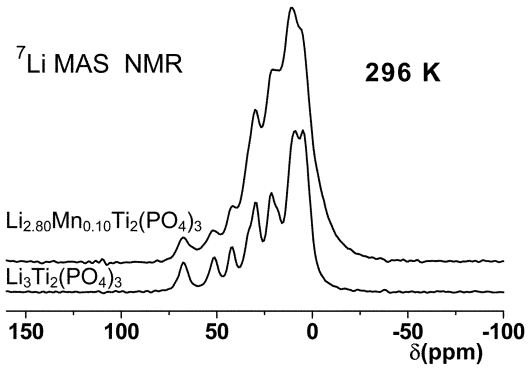

Fig. 12 Comparison between the ^{7}Li MAS NMR spectrum of $Li_3Ti_2(PO_4)_3$ and that of $Li_{2.80}Mn_{0.10}Ti_2(PO_4)_3$.

Conclusion

This study shows a satisfactory agreement between neutron and XRD data on the one hand and ^{7}Li NMR data on the other hand for $Li_3Ti_2(PO_4)_3$, showing that Li occupies the M3 and M′3 sites within the M2 cavity. This leads to a distribution of ^{7}Li NMR signals, due to the effect of the relative number of M3 and M′3 sites occupied around a given M3 or M′3 site. Hopping between the two positions is evidenced and leads to an exchanged ^{7}Li NMR signal at 353 K, whereas diffraction sees a statistical occupation of the two sites both at RT and at 350 K, due to its fast time scale.

It is however important to note that relatively satisfactory Rietveld refinements of the X-Ray and neutron diffraction patterns were also obtained with a single position for Li^+ ions (M3). However, this is not compatible with the observed distribution of ^{7}Li NMR signals, so that the neutron diffraction analysis was carefully reconsidered, and led to occupation by lithium of the two available M3 and M′3 sites. It is also worth noting that a slightly faster exchange between the two sites might have led to an exchanged NMR signal at room temperature, thus providing no evidence for the occupation of several sites.

References

1 H. P. Y. Hong, *Mater. Res. Bull.*, 1976, **11**, 173.
2 J. B. Goodenough, H. Y. P. Hong and J. A. Kafalas, *Mater. Res. Bull.*, 1981, **11**, 285.
3 F. D'Yvoire, M. Pintard-Screpel, E. Bretey and M. G. de la Rochere, *Solid State Ionics*, 1983, **9/10**, 851.
4 R. Roy, D. K. Agrawal, J. Alamo and R. A. Roy, *Mater. Res. Bull.*, 1984, **19**, 471.
5 T. Maruyama, S. Sasaki and Y. Saito, *Solid State Ionics*, 1987, **23**, 107.
6 M. Catti, S. Stramare and R. Ibberson, *Solid State Ionics*, 1999, **123**, 173.
7 F. Cherkaoui, J. C. Viala, C. Delmas and P. Hagenmuller, *Solid State Ionics*, 1986, **21**, 333.
8 C. Delmas, F. Cherkaoui, A. Nadiri and P. Hagenmuller, *Mater. Res. Bull.*, 1987, **22**, 631.
9 O. Tillement, J. C. Couturier, J. Angenault and M. Quarton, *Solid State Ionics*, 1991, **48**, 249.
10 J. B. Goodenough, *Mol. Cryst. Liq.Cryst.*, 1998, **311**, 409.
11 A. K. Padhi, K. S. Nanjundaswamy, C. Masquelier and J. B. Goodenough, *J. Electrochem. Soc.*, 1997, **144**(8), 2581.
12 D. Petit, Ph. Colomban, G. Collin and J. P. Boillot, *Mater. Res. Bull.*, 1986, **21**, 365.
13 L. O. Hagman and P. Kierkegaard, *Acta Chem. Scand.*, 1986, **22**, 1822.
14 J. P. Boilot, G. Collin and Ph. Colomban, *Mater. Res. Bull.*, 1987, **22**, 669.
15 J. P. Boilot, G. Collin and Ph. Colomban, *J. Solid State Chem.*, 1988, **73**, 160.
16 O. Tillement, J. Angenault, J. C. Couturier and M. Quarton, *Solid State Ionics*, 1992, **53–56**, 391.
17 C. Masquelier, A. K. Padhi, K. S. Nanjundaswamy and J. B. Goodenough, *J. Solid. State Chem.*, 1998, **135**, 228.
18 C. Masquelier, C. Wurn, J. Rodriguez-Carvajal, J. Gaubicher and L. Nazar, *Chem. Mater.*, 2000, **12**, 525.
19 J. Gaubicher, C. Wurn, G. Goward, C. Masquelier and L. Nazar, *Chem. Mater.*, 2000, **12**, 3240.
20 C. Delmas, A. Nadiri and J. L. Soubeyroux, *Solid State Ionics*, 1988, **28–30**, 419.
21 A. Aatiq, C. Delmas, A. El Jazouli and P. Gravereau, *Ann. Chim. Sci. Mater.*, 1998, **23**, 121.
22 A. Aatiq, C. Delmas and A. El Jazouli, *J. Solid. State Chem.*, 2001, **158**, 169.
23 A. K. Padhi, K. S. Nanjundaswamy and J. B. Goodenough, *J. Electrochem. Soc.*, 1997, **144**, 1188.
24 N. Ravet, J. B. Goodenough, S. Besner, M. Simoneau, P. Hovington and M. Armand, in *Abstracts of the ECS Fall Meeting, Honolulu, Hawaii, October 1999*, Electrochemical Society, Pennington, NJ, 1999, abstr. 127.
25 H. Huang, S. C. Yin and L. F. Nazar, *Electrochem. Solid-State Lett.*, 2001, **4**(10), A170.
26 M. Morcrette, C. Wurm, J. Gaubicher and C. Masquelier, in *Abstracts of the Lithium Battery Discussion Meeting (LiBD 2001), Arcachon, France*, ed. C. Delmas, 2001, abstr. 98.
27 H. Fakrane, A. Aatiq, M. Lamire, A. El Jazouli and C. Delmas, *Ann. Chim. Sci. Mater.*, 1998, **23**, 81.
28 A. Aatiq, M. Ménetrier, A. El Jazouli and C. Delmas, *Solid State Ionics*, 2002, **150**(3–4), 391–405.
29 A. Aatiq, PhD Thesis, Faculty of Science Ben M'Sik, Casablanca, Morocco, 1997.
30 A. Boireau, J. L. Soubeyroux, R. Olazcuaga, C. Delmas and G. Le Flem, *Solid State Ionics*, 1993, **63–65**, 484.
31 P. R. Slater and C. Greaves, *J. Mater. Chem.*, 1994, **4**(9), 1463.
32 A. Mendiboure and C. Delmas, *Comput. Chem.*, 1987, **11**(3), 153.
33 J. Rodriguez-Carvajal, FullProf, Program for Rietveld Refinement, Laboratoire Léon Brillouin (CEA-CNRS), Saclay, France, 1997.
34 R. D. Shannon, *Acta Crystallogr., Sect. A*, 1976, **32**, 751.
35 M. Alami, R. Brochu, J. L. Soubeyroux, P. Gravereau, G. Le Flem and P. Hagenmuller, *J. Solid. State Chem.*, 1991, **90**, 185.